AIAA JOURNAL
Vol. 34, No. 6, June 1996

# Use of the Energy Flow Concept in Vibration Design

K. S. Alfredsson,* B. L. Josefson,† and M. A. Wilson*
*Chalmers University of Technology, S-412 96 Göteborg, Sweden*

**Stationary harmonic vibration of damped elastic structures is studied. Energy flow in structures is calculated using results from ordinary harmonic response finite element analyses. In two examples both global and local quantities, such as the supplied power and the mechanical intensity, are calculated and displayed. Both proportionally and nonproportionally damped structures are studied. The magnitude of the real part of the mechanical intensity is, in the examples, seen to have roughly the same spatial distribution as the strain energy density. The potential use of the mechanical intensity as a tool for identifying transmission paths for energy is demonstrated.**

## Nomenclature

$\boldsymbol{a}$ = real part of mechanical intensity vector
$B$ = imaginary part of mobility matrix
$C$ = damping matrix
$\boldsymbol{c}$ = complex mechanical intensity vector
$E$ = dynamic stiffness matrix
$e$ = dynamic flexibility matrix
$\boldsymbol{F}$ = force vector
$f$ = frequency
$G$ = real part of mobility matrix
$L$ = supplied power
$M$ = mass matrix
$m$ = point mass
$P$ = real part of supplied power
$Q$ = imaginary part of supplied power
$\boldsymbol{q}$ = mechanical intensity vector
$\boldsymbol{r}$ = imaginary part of mechanical intensity vector
$S$ = supplied complex power
$T$ = kinetic strain energy
$U$ = elastic strain energy
$V$ = volume
$\boldsymbol{v}$ = velocity vector
$W$ = stored power
$\boldsymbol{X}$ = nodal degrees of freedom vector
$\boldsymbol{Y}$ = mobility matrix
$\eta$ = stiffness proportional damping loss factor
$\theta$ = mass proportional damping loss factor
$\lambda^G_{\min}$ = lowest eigenvalue of matrix $G$
$\lambda^G_{\max}$ = largest eigenvalue of matrix $G$
$\Pi$ = dissipated power
$\sigma$ = stress tensor
$\omega$ = angular frequency

*Subscripts*

$i$ = direction $i$
0 = per unit volume
$\infty$ = infinitely long beam
$\_$ = complex entity

*Superscripts*

$H$ = Hermitian transpose
$*$ = complex conjugate
$\bar{}$ = time average

Presented as Paper 95-1497 at the AIAA/ASME/ASCE/AHS/ASC 36th Structures, Structural Dynamics, and Materials Conference, New Orleans, LA, April 10–12, 1995; received July 6, 1995; revision received Jan. 16, 1996; accepted for publication Jan. 16, 1996. 

*Graduate Student, Division of Solid Mechanics.
†Professor, Division of Solid Mechanics. Member AIAA.

## Introduction

THE demand for noise reduction in vehicles like cars, trucks, trams, and airplanes will most likely increase in the near future. Structure borne sound constitutes a special problem and must be considered early in the design process since low-frequency sound transmission is difficult to reduce in an existing structure. In this context it is desirable to obtain a qualitative knowledge of dominant paths of energy transfer in the structure of interest.

Two examples of experimental work demonstrating the potential use of the energy flow concept are given by Verheij et al.[1] and Bohineust et al.[2] In Ref. 1 the primary energy transmission path in a ship structure, from the excitation source (gearbox, shaft, and propeller) to areas with strong radiation of sound, is identified. In Ref. 2 the energy flowfield in the rear floor of a car is studied to find the best location for additional damping material.

Knowledge of energy transmission paths in dynamically loaded structures may also be obtained by use of computational methods. For low frequencies, the finite element (FE) method is a powerful tool, which provides calculated displacement and velocity fields and eigenmodes with sufficient accuracy. The approximation normally made in a dynamic FE analysis to discretize the inertia forces and to use polynomial shape functions for the assumed displacement field will be reasonably good. Energy-based methods, such as statistical energy analysis, are, on the other hand, difficult to apply because of the low modal density at low frequencies. Results from FE-based harmonic response analyses may be used to extract information about energy flowfields. Energy flow is mathematically described with the mechanical intensity vector $\boldsymbol{q}_i = -\sigma_{ij}\boldsymbol{v}_j$. The mechanical intensity vector field contains information about the direction and magnitude of the rate of energy flow (power flow) per unit cross-sectional area and may be displayed as an image of the energy flowfield. With a proper modeling of potential energy sinks, such as internal damping or additional layers of damping material, transmission paths for the energy in the structure, as modeled by the time average of $\boldsymbol{q}_i$, can be calculated and displayed.

Predictions and visualizations of energy flow based on ordinary displacement based FE analyses have been provided in Refs. 3–7. In Hambric,[3,4] formulas for energy flow have been implemented into the commercial FE-code NASTRAN, whereas in Gavric and Pavic,[5] intensity fields are calculated by use of an in-house code employing undamped eigenmodes. Alfredsson[6,7] presents a thorough derivation of intensity fields present in damped elastic solids performing stationary harmonic vibration. Formulas derived in Alfredsson[6,7] have been implemented into the commercial FE-code SOLVIA.[8]

In this paper, the computational approach is applied to two problems of technical interest. First, a machine mounted on a portal frame is studied. The portal frame, in turn, is placed on a foundation modeled as a beam. Different kinds of foundations are modeled by using a finite and an infinite beam, respectively. The second example considers the local energy flow in a builtup shell structure. The shell structure consists of a set of flexible plates mounted inside a flexible cylinder. Both global quantities, such as the power supplied to the structure, and local quantities, such as the mechanical intensity

inside the structure, are calculated and displayed. Relations between the supplied power and the total elastic strain energy of the structure are demonstrated. The issue of finding appropriate design measures to quantify vibration levels is also addressed.

## Basic Equations

Consider an elastic solid subjected to time-varying external loads. A linear viscoelastic material model of Kelvin type is used to describe internal hysteretic material damping quantified with a loss factor $\eta$. Defining the instantaneous mechanical intensity as $q_i = -\sigma_{ij} v_j$, the energy continuity equation will read (see Ref. 6)

$$\dot{W}_0 + \Pi_0 = L_0 - q_{i,i} \tag{1}$$

Equation (1) expresses a mechanical power balance for an infinitesimal volume. The left-hand side contains the power $\dot{W}_0$ being stored, that is, the change in total reversible energy (sum of strain and kinetic energies) and the power $\Pi_0$ being dissipated inside the volume. The right-hand side contains the power $L_0$ supplied per unit volume by external body forces and the power $-q_{i,i}$ flowing into the infinitesimal volume through its boundaries.

For the case of stationary harmonic vibration at a given frequency $\omega$, the complex mechanical intensity $\underline{c}_i$ is introduced:

$$\underline{c}_i = -\tfrac{1}{2}\underline{\sigma}^*_{ij}\underline{v}_j = a_i + ir_i \tag{2}$$

The real part $a_i$ of the complex mechanical intensity is termed the active mechanical intensity and corresponds to the net (average) energy flow rate per unit cross-sectional area. The imaginary part $r_i$ is called the reactive mechanical intensity.

Introducing the complex power supplied per unit volume by body forces, $\underline{S}_0 = P_0 + iQ_0$, the continuity equations for the active and reactive intensities may be written

$$a_{i,i} = P_0 - \Pi_0 \tag{3a}$$

$$r_{i,i} = Q_0 - 2\omega(\bar{U}_0 - \bar{T}_0) \tag{3b}$$

Here $\bar{\Pi}_0$, $\bar{U}_0$, and $\bar{T}_0$ are the time-averaged power dissipated per unit volume, the elastic strain energy density, and the kinetic energy density, respectively.

For the complete structure one may define the total complex power, $\underline{S} = P + iQ$, supplied by all external loads, that is, both body forces and boundary loads. Balances prevail between supplied active power $P$ and the dissipated power $\Pi$ on one hand, and the supplied reactive power $Q$ and the total strain and kinetic energies $U$ and $T$ on the other hand,

$$P = \bar{\Pi} \tag{4a}$$

$$Q = 2\omega(\bar{U} - \bar{T}) \tag{4b}$$

Hence, the total supplied active power equals the time average of the total power dissipated in the structure. The reactive power is related to the difference between the time averages of the strain and kinetic energies.

The discretization of the structure into displacement based finite elements will lead to a system of ordinary differential equations

$$M\ddot{X} + C\dot{X} + KX = F \tag{5}$$

The unknown nodal degrees of freedom (DOFs) (translations and cross-sectional rotations) are collected in the column vector $X$ and the nodal loads are collected in the column vector $F$. For stationary harmonic vibration the linear system of equations, Eq. (5), can be solved by matrix inversion using complex arithmetic:

$$\underline{X} = \underline{e}\,\underline{F} \tag{6}$$

$$\underline{e} = (K + i\omega C - \omega^2 M)^{-1} \tag{7a}$$

$$C = (\eta/\omega)K \tag{7b}$$

For a discretized system the total complex power supplied is

$$\underline{S} = \tfrac{1}{2}\underline{F}^H\underline{X} = P + iQ \tag{8}$$

The average power dissipated and the average strain and kinetic energies are for a discretized system given by

$$\bar{\Pi} = \tfrac{1}{2}\underline{\dot{X}}^H C\underline{\dot{X}} \tag{9a}$$

$$\bar{U} = \tfrac{1}{4}\underline{X}^H K\underline{X} \tag{9b}$$

$$\bar{T} = \tfrac{1}{4}\underline{\dot{X}}^H M\underline{\dot{X}} \tag{9c}$$

The balance Eqs. (4a) and (4b) are valid also for the discretized system with $P$, $Q$, $\bar{\Pi}$, $\bar{U}$, and $\bar{T}$ given by Eqs. (8) and (9a–9c).

For a vibrating structure subjected to loads with harmonic time dependence, the supplied power will vary with frequency, location, and phase relations of the exciting loads. The active and reactive supplied power can be expressed in structural and loading properties as

$$P = \tfrac{1}{2}\underline{F}^H G\underline{F} \tag{10a}$$

$$Q = \tfrac{1}{2}\underline{F}^H B\underline{F} \tag{10b}$$

where $G$ and $B$ are defined by

$$\underline{Y} = i\omega\underline{e} = G + iB \tag{11}$$

It is possible to establish the following bounds for the active power[6]:

$$\lambda^G_{\min}|\underline{F}|^2 \le 2P \le \lambda^G_{\max}|\underline{F}|^2 \tag{12a}$$

$$|\underline{F}|^2 = \underline{F}^H\underline{F} \tag{12b}$$

where $\lambda^G_{\min}$ and $\lambda^G_{\max}$ are the lowest and largest eigenvalues of $G$ (the real part of the mobility matrix $\underline{Y}$). These limits can be used to investigate the frequency dependence of $P$. In Alfredsson[6] it was observed in numerical examples that load vectors supplying the maximum active power was nearly identical to the eigenmode corresponding to the closest eigenfrequency. A load vector that supplies minimum active power should be collinear with the eigenvector of $G$ corresponding to the lowest eigenvalue $\lambda^G_{\min}$.

## Numerical Examples

The theory referred to will now be used in two examples.

### Global Energy Flow in Frame on Foundation

In the first example a plane frame structure is studied; see Fig. 1. This structure should resemble a machine (rigid mass) mounted on a portal frame, which in turn is placed on a horizontal foundation. The structure is built up from 10 standard two-node beam elements (Euler–Bernoulli theory) with cubic interpolation functions for the transverse displacement and linear interpolation functions for the axial displacement. Consistent mass matrices are employed. The structure is first simply supported in two points on the foundation. The rigid mass is excited by a rotating imbalance, that is, two perpendicular forces (both being proportional to $\omega^2$) with a mutual

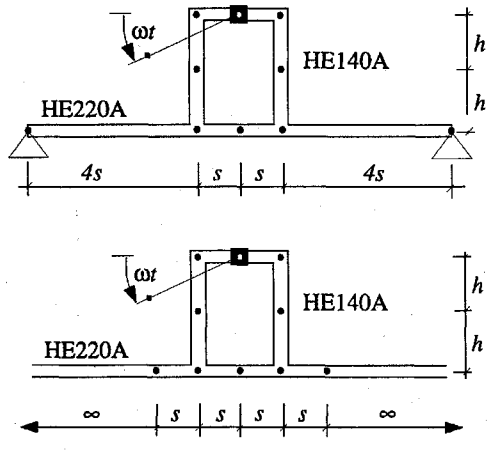


**Fig. 1 Geometry of plane frame structure; upper part shows simply supported foundation and lower part shows infinite foundation.**

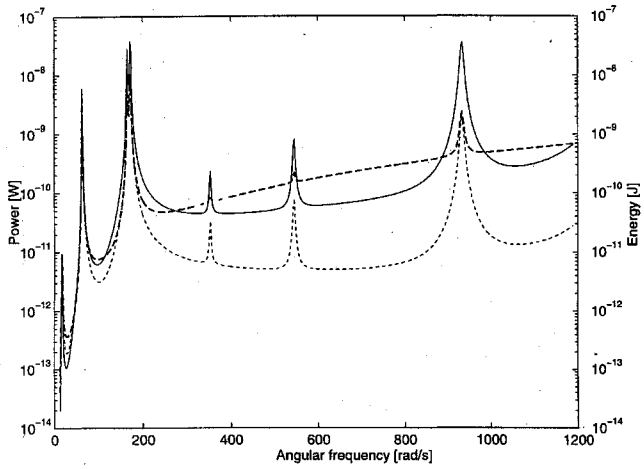


**Fig. 2 Calculated frequency variation of active power, strain energy, and kinetic energy; proportionally damped structure: ——, active power $P$; - - - - -, strain energy $\bar{U}$; and – – –, kinetic energy $\bar{T}$.**

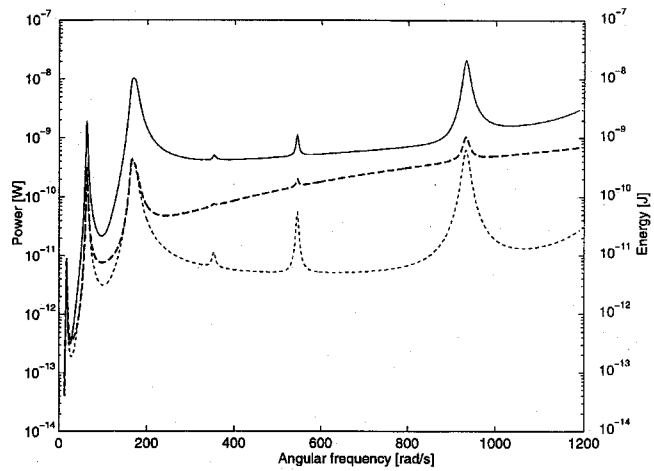


**Fig. 3 Calculated frequency variation of active power, strain energy, and kinetic energy when structure is nonproportionally damped: ——, active power $P$; - - - - -, strain energy $\bar{U}$; and – – –, kinetic energy $\bar{T}$.**

phase angle 90 deg. This example was first studied in Schill.[9] Here the structure is taken as proportionally damped with the loss factor $\eta = 0.01$. All other values for lengths and tensile and bending stiffnesses are taken from Schill.[9] The results presented for this example have been obtained from a small in-house code using MATLAB™. Figure 2 shows the calculated variation with $\omega$ for the supplied power $P$ and the time average of the elastic strain energy $\bar{U}$ and kinetic energy $\bar{T}$.

The supplied power is an interesting entity in vibration isolation problems. The aim is to optimize the isolator design so that the power flowing into the structure is minimized. This will also minimize the power available for subsequent radiation and vibration.

One finds that $\bar{U}$ has a similar $\omega$ variation as the supplied power $P$, whereas the kinetic energy has a somewhat different frequency variation. Indeed, it is straightforward to show by use of Eqs. (6–8) that, for a structure with stiffness proportional damping [see Eq. (7b)], the active power is proportional to the elastic strain energy [see also Eq. (4a)]:

$$P = 2\eta\omega\bar{U} \tag{13a}$$

If one instead postulates that the damping is hysteretic but mass proportional with a loss factor $\theta$, the corresponding relation will be

$$P = 2(\theta/\omega)\bar{T} \tag{13b}$$

The possible proportionality between $P$ and energy measures has also been discussed in Pavic.[10] He, however, tried to establish a relation between $P$ and $\bar{T}$ using mode superposition. The relationship, Eq. (13a), is found to hold also approximately if the structure becomes nonproportionally damped. By changing the loss factor to $\eta = 0.15$ for the portal frame, one obtains the corresponding calculated variation with $\omega$ for the supplied power $P$ and the time average of the elastic strain energy $\bar{U}$ shown in Fig. 3. It is seen in Fig. 3 that there seems to be a reasonable proportionality between $P$ and $\bar{U}$.

Figure 4 shows the application of the bounds for $P$ given by Eq. (12a) for the nonproportionally damped structure. The appearance of the bounds in Eq. (12a) is clearly displayed in Fig. 4. The maximum and minimum eigenvalues of $G$ are calculated by use of inverse and forward iteration,[11] respectively. The size of $G$ and its eigenvectors is determined by the number of DOF, that is, the size of $\underline{F}$. Note, however, that when evaluating the eigenvalues for the real part of the mobility matrix $G$, the size of $G$ can be reduced by eliminating the rows and columns corresponding to DOFs that do not carry loads. From the Sturm sequence property,[11] it follows that the lowest eigenvalue is generally raised and the highest eigenvalue lowered when a row and column are deleted from $G$. The bounds, for the present case with only two nonzero components in the load vector will then be located close to the $P$ curve. Note, though, that the curves shown in Fig. 4 are calculated using the full matrix $G$.

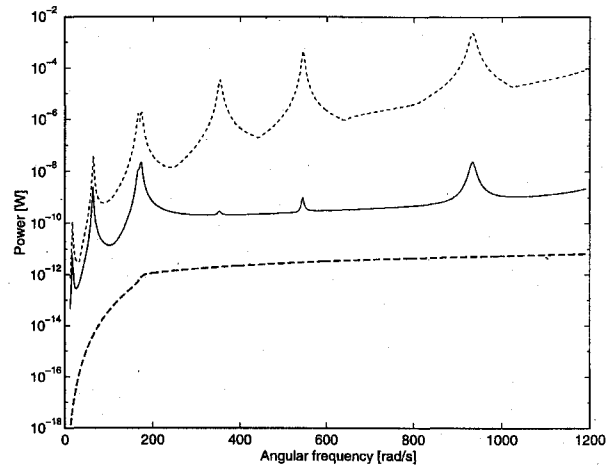


**Fig. 4 Calculated frequency variation of $P$, and upper and lower bounds for $P$: ——, active power $P$; - - - -, upper bound $\bar{U}$; and – – –, lower bound $\bar{T}$.**

Note also that use of the bounds in Eq. (12a) requires the inversion of the dynamic stiffness matrix, Eq. (7a). However, the bounds in Eq. (12a) can be used to investigate the possible variation of the active power for different load vectors.

Consider now the case when the supports are removed and the lower horizontal foundation is taken as infinitely long, see Fig. 1. The semi-infinite parts of the foundation are then modeled by one-node semi-infinite beam elements. The dynamic stiffness matrix $E_\infty$ associated with this element (Euler–Bernoulli theory is assumed) is derived by calculating end forces needed to displace and rotate the end of the semi-infinite beam, see also Refs. 9 and 12. Hence, the total global flexibility matrix can be obtained as (for harmonic loading)

$$\underline{e} = \left(K + i\omega C - \omega^2 M + E_\infty\right)^{-1} \tag{14}$$

Note that $E_\infty$ contains both stiffness, internal damping, and mass properties for the semi-infinite beams. For a given response $\underline{X}$, the stored elastic strain energy $\bar{U}$ and kinetic energy $\bar{T}$ for the semi-infinite beams are calculated separately and added to the previously derived expressions for $\bar{U}$ and $\bar{T}$, Eqs. (9b) and (9c). One finds, for example, that for a semi-infinite beam $Q \neq 2\omega(\bar{U} - \bar{T})$ relation Eq. (4b) for the reactive power will no longer hold. Figure 5 shows the calculated variation with $\omega$ for the supplied power $P$ and the time average of the elastic strain energy $\bar{U}$ and the time average of the kinetic energy $\bar{T}$ for the semi-infinite foundation case.

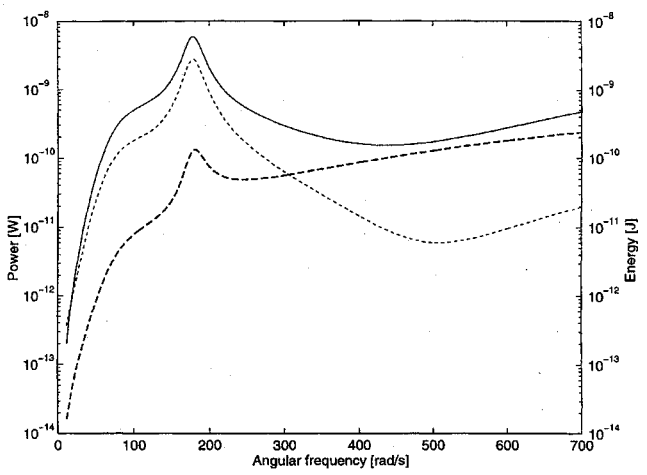


**Fig. 5 Calculated frequency variation of active power, strain energy, and kinetic energy for structure with infinite foundation: ——, active power $P$; - - - -, strain energy $\bar{U}$; and – – –, kinetic energy $\bar{T}$.**

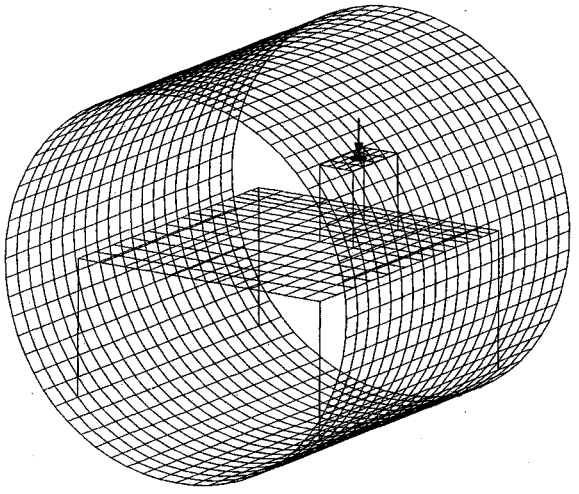

**Fig. 6 FE mesh used for builtup shell structure; cylinder length = 1.4 m, radius = 0.35 m; point mass on upper plate is loaded with vertical force.**

### Local Energy Flow in Builtup Shell Structure

In the second example, a builtup shell structure is studied. A point mass is placed on a horizontal flexible (upper) plate, which, in turn, is connected to a larger horizontal (lower) plate through four vertical springs. This lower plate is connected to the inner side of a flexible circular cylinder (also) through four vertical springs. The FE mesh used for the structure is shown in Fig. 6. The structure consists of some 1560 four-node shell elements,[13] employing consistent mass matrices, and eight spring elements resulting in totally 9200 complex valued DOFs. The geometry in this example has been designed to be similar to the one presented in Pan and Hansen,[14] where vibratory power transmission from a rigid body through a flexible support is studied semianalytically. The simplified structure in this example and in Pan and Hansen[14] should represent a typical submarine application. Some dimensions, such as those for the circular cylinder, have been taken the same as in the shell structure studied in Pan and Hansen.[14] This means that wall thicknesses are taken as 5–10 mm. The length of the cylinder is 1.4 m and the radius of the cylinder is 0.35 m. Note that the upper plate is placed eccentrically on the lower plate in both horizontal directions.

The shell structure is initially proportionally damped with the loss factor taken as $\eta = 0.01$ (except for the springs, which have a viscous damping factor chosen to give the same damping as the given loss factor at the frequency studied). It is loaded by a vertical harmonic point force at the rigid mass. Figures 7a and 7b show the calculated magnitude of active intensity $|\boldsymbol{a}_i|$ (left) and time average

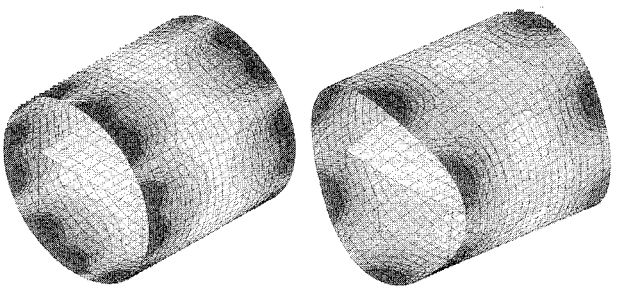

**Fig. 7a Calculated magnitude of active intensity $|a_i|$, left, and time average of elastic strain energy density $\bar{U}_0$, right, in shell structure at $f = 45$ Hz.**

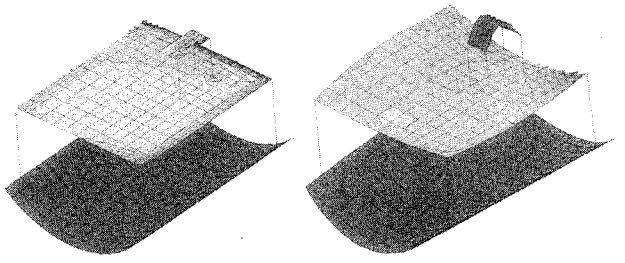

**Fig. 7b Calculated magnitude of active intensity $|a_i|$, left, and time average of elastic strain energy density $\bar{U}_0$, right, in upper and lower plates of shell structure at $f = 45$ Hz.**

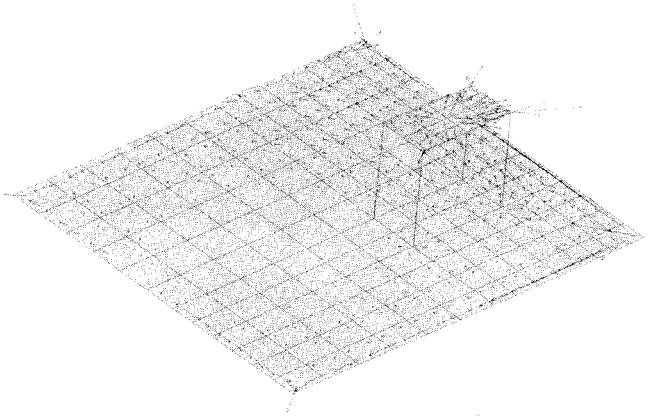

**Fig. 8 Calculated vector field $a_i$ in upper and lower plates at $f = 45$ Hz.**

of elastic strain energy density $\bar{U}_0$ (right) in the structure at one resonance frequency, $f = 45$ Hz. The real part of this resonance mode, which is displayed to the right in Figs. 7a and 7b, excites all parts of the structure.

Dark areas indicate higher values for $|\boldsymbol{a}_i|$ and $\bar{U}_0$. One finds the spatial variation of $|\boldsymbol{a}_i|$ and $\bar{U}_0$ to be similar, although the direction of the active intensity is not displayed. Note that the results displayed in Figs. 7a and 7b are taken from the same computation, but that different levels have been used for the contour surfaces to obtain a higher resolution in Fig. 7b. As seen in Fig. 7a both the active intensity and the strain energy density is much larger in parts of the cylinder than in the plates. Figure 8 shows the calculated vector field $\boldsymbol{a}_i$ in the upper and lower horizontal plates (at the same frequency). It is seen that the energy flow through the four springs to the lower plate and to the cylinder is not uniform; on the contrary most of the energy is transmitted through one particular spring.

The spatial variation of the active intensity $\boldsymbol{a}_i$ will strongly depend on the damping of the structure as indicated by Eq. (3a).

Figure 9 shows the calculated vector field $\boldsymbol{a}_i$ at the frequency 36 Hz in the plates for the case when the loss factor $\eta = 0.1$ and when the stiffness of the springs is decreased to $\frac{1}{100}$ of the value used for Figs. 7 and 8. At this frequency the modified structure has a resonance frequency corresponding to the one at 45 Hz for the original structure. It is clearly seen that the vector field has a

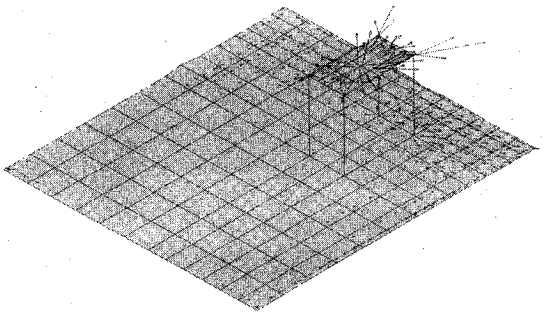

**Fig. 9 Calculated vector field $a_i$ in upper and lower plates at $f = 36$ Hz; structure has increased loss factor of 10 and decreased spring stiffnesses factor of 100.**

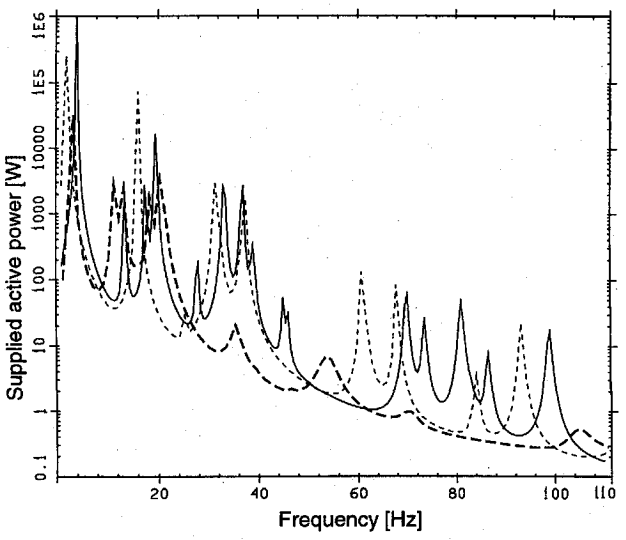


**Fig. 10 Calculated frequency variation of supplied active power for shell structure: ——, stiffness $K$; – – –, stiffness $k/100$; and - - - -, stiffness $k$, dynamic condensation.**

different shape and that the energy flow is different from the one in Fig. 8. This difference in shape and magnitude for $a_i$ is a result of the modifications of both damping and spring stiffness.

Figure 10 shows the calculated frequency variation of the supplied active power at the point mass (where the vertical point force is applied). One finds that several eigenmodes are excited, with the lowest excited one corresponding to a local vertical translation of (the central part of) both plates and their support springs. By reducing the spring stiffnesses by a factor of 100, the supplied power will decrease for lower frequencies. This was also found in Pan and Hansen.[14] As seen in Fig. 10, however, at some higher frequencies, the supplied power may increase.

To save computer time, dynamic substructuring is often employed in dynamic FE analyses. Included in Fig. 10 is the corresponding frequency variation when dynamic substructuring, or rather dynamic condensation, using Guyan reduction[11] has been used (with springs having the original stiffness). Hence, the structure stiffness and mass matrices for the cylinder are reduced using static condensation, that is, neglecting inertia forces on slave DOFs when establishing a relation between master DOFs and slave DOFs. The four connection points for the vertical springs are chosen as points with master DOFs. Moreover, the cylinder is taken as undamped and the plates and springs are given the loss factor $\eta = 0.01$. One finds, as expected, that all eigenmodes of the original structure will not be excited and that some resonance frequencies have been altered.

Choosing only connection DOFs as master DOFs is normally considered to give an inaccurate solution. One would normally add some extra master DOFs or include internal eigenmodes for the substructure. However, because the connection DOFs are located

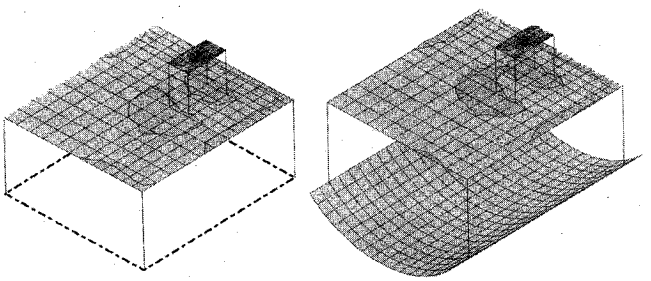

**Fig. 11 Calculated magnitude of active intensity $|a_i|$ in plates for normal case (right) and for case with dynamic condensation (left) at $f = 16$ Hz.**

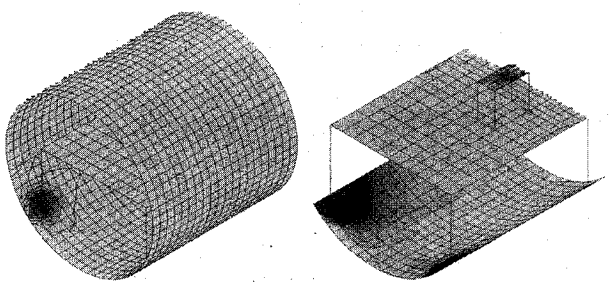

**Fig. 12 Calculated magnitude of active intensity $|a_i|$ in structure when cylinder ends have shear diaphragm boundary conditions; frequency $f = 45$ Hz.**

at different parts of the cylinder at zones, which contribute to the deformation at the specific frequency, the present choice may be justified for this simple example.

The sensitivity in the calculated solution for the energy flow may be investigated by studying effects of dynamic substructuring at a resonance frequency, which is excited in the substructure case. Figure 11 compares the magnitude of the active intensity $|a_i|$ at 16 Hz in the plates as calculated for the complete structure (right) and as calculated using dynamic substructuring (left) where the cylinder has been condensed. It is seen in Fig. 11 that the active intensity field in the plates can be modeled accurately when dynamic substructuring is employed.

In the calculations behind Figs. 7–11 the cylinder has free ends. This means that the cylinder ends will deflect considerably at some resonance frequencies, which will result in high values for $|a_i|$ and $\bar{U}_0$ at the cylinder ends. The structure studied in Pan and Hansen[14] has shear diaphragm boundary conditions at the cylinder ends. Figure 12 shows the calculated magnitude of the active intensity $|a_i|$ in the cylinder at $f = 19$ Hz for a modified structure with shear diaphragm boundary conditions for the cylinder ends. This resonance frequency for the modified structure will give roughly the same deflections, in parts of the structure other than at the cylinder ends, as the resonance frequency $f = 45$ Hz for the original structure. Compared to Figs. 7a and 7b the magnitude of the active intensity is seen to have roughly the same spatial variation in the plates.

## Discussion

For proportionally damped structures, a relationship between the supplied power $P$ and the time average of strain energy $\bar{U}$ can be established. This proportionality was found to hold approximately also when the structure is nonproportionally damped. The calculations show that the two local quantities, the magnitude of the active intensity $|a_i|$ and the strain energy density $\bar{U}_0$, will have fields with similar shape both when the structure is proportionally damped and when the structure is nonproportionally damped [that is, Eq. (7b) holds only on the element level]. However, studying the active intensity field $a_i$ will give more information than the scalar entity elastic strain energy density $\bar{U}_0$ since information about the direction of the energy flow will also be provided.

It remains, however, to determine how to display the vector field $a_i$. In SOLVIA,[8] the mechanical intensity $\underline{c}_i$ is evaluated from stresses calculated in the appropriate Gaussian integration points

and from nodal velocities calculated at nodes and interpolated to the integration points. Note that the damping enters both in the discretized system of the FE equations [Eq. (5)] when calculating $v_j$ and in the constitutive equation when calculating $\sigma_{ij}$. The mechanical intensity is then displayed at the Gaussian integration points. A relatively fine mesh is needed with this approach to ensure a reasonably continuous stress field, that is, to reduce jumps in stresses in adjacent elements that share nodes. On the other hand, use of a fine element mesh will result in an extensive amount of information in each element. Some condensation, or averaging, of the information presently provided might then be needed before the vector field is displayed.

This paper has focused on the active (real) part of the mechanical intensity and supplied power. As discussed, this real part of these entities has a specific physical interpretation. It is more difficult to interpret the reactive part of the mechanical intensity and supplied power. The appearance of these reactive parts $r_i$ and $Q$ has been discussed by Alfredsson[6,7] and by other authors, for example, Maysenhölder.[15] Similarities and differences for the reactive parts of the intensity in fluids and in solids are also disussed in these references. Their conclusion is that there seems to be no obvious practical use for the reactive parts of the mechanical intensity and supplied power.

## Acknowledgment

The work presented here was funded by the Swedish Research Council for Engineering Sciences through Contract 94-300.

## References

[1]Verheij, J. W., Hopmans, L. J. M., and van Tol, F. H., "Shipboard Measurements of Structural Intensity on a Rotating Shaft and Its Use for Sound Path Quantification," *Structural Intensity and Vibrational Energy Flow*, edited by G. Pavic, Proceedings of the 4th International Congress on Intensity Techniques, CETIM, Senlis, France, 1993, pp. 423–429.

[2]Bohineust, X., Bouizem, B., and Stawicki, C., "Vibration Ranking of Multy Path Energy Transfer in Vehicle Structures Using Structural Intensity Measurement," *Structural Intensity and Vibrational Energy Flow*, edited by G. Pavic, Proceedings of the 4th International Congress on Intensity Techniques, CETIM, Senlis, France, 1993, pp. 437–444.

[3]Hambric, S. A., "Power Flow and Mechanical Intensity Calculations in Structural Finite Element Analysis," *Journal of Vibration and Acoustics*, Vol. 112, No. 4, 1990, pp. 542–549.

[4]Hambric, S. A., "Visualization of Structure-Borne Power in Finite Element Plate Models," *Inter-Noise 92*, edited by G. A. Daigle and M. R. Stinson, Proceedings of the 1992 International Congress on Noise Control and Engineering, Vol. 1, Noise Control Foundation, Poughkeepsie, NY, 1992, pp. 533–536.

[5]Gavric, L., and Pavic, G., "A Finite Element Method for Computation of Structural Intensity by the Normal Mode Approach," *Journal of Sound and Vibration*, Vol. 164, No. 1, 1993, pp. 29–43.

[6]Alfredsson, K. S., "Active and Reactive Structural Energy Flow," *Journal of Vibration and Acoustics* (to be published).

[7]Alfredsson, K. S., "Influence of Local Damping on Active and Reactive Mechanical Power Flow," *Structural Intensity and Vibrational Energy Flow*, edited by G. Pavic, Proceedings of the 4th International Congress on Intensity Techniques, CETIM, Senlis, France, 1993, pp. 71–78.

[8]Anon., "SOLVIA-PRE 95.0—User's Manual," SOLVIA Engineering, Västerås, Sweden, 1995.

[9]Schill, M., "Damped Second-Order Rayleigh–Timoshenko Semi-Infinite Beam Vibration—An Exact Complex Dynamic Member Stiffness Matrix," *International Journal for Numerical Methods in Engineering*, Vol. 26, No. 8, 1988, pp. 1893–1905.

[10]Pavic, G., "On the Relationship Between the Energy Flow Into a Structure and Its Vibration," *Structural Intensity and Vibrational Energy Flow*, edited by G. Pavic, Proceedings of the 4th International Congress on Intensity Techniques, CETIM, Senlis, France, 1993, pp. 95–99.

[11]Bathe, K.-J., *Finite Element Procedures*, Prentice–Hall, Englewood Cliffs, NJ, 1996.

[12]Gavric, L., "Power-Flow Analysis Using Infinite Beam Elements," *Journal de Physique IV, Colloque C1*, Vol. 2, No. C1, 1992, pp. C1-511–C1-514.

[13]Bathe, K.-J., and Dvorkin, E. N., "A Four-Node Plate Bending Element Based on Mindlin/Reissner Plate Theory and a Mixed Interpolation," *International Journal of Numerical Methods in Engineering*, Vol. 21, No. 2, 1985, pp. 367–383.

[14]Pan, J., and Hansen, C. H., "Power Transmission from a Vibrating Source Through an Intermediate Flexible Panel to a Flexible Cylinder," *Journal of Vibration and Acoustics*, Vol. 116, No. 4, 1994, pp. 496–505.

[15]Maysenhölder, W., "The Reactive Intensity of General Time-Harmonic Structure-Borne Sound Fields," *Structural Intensity and Vibrational Energy Flow*, edited by G. Pavic, Proceedings of the 4th International Congress on Intensity Techniques, CETIM, Senlis, France, 1993, pp. 63–70.